CTNND2 moderates neuronal excitation and links human evolution to prolonged synaptic development in the neocortex

Nora Assendorp[1], Marine Depp[1], Matteo Fossati[1,2], Florent Dingli[3], Damarys Loew[3] and Cécile Charrier[1#]

[1] Institut de Biologie de l'ENS (IBENS), Ecole Normale Supérieure, CNRS, INSERM, PSL Research University, 75005 Paris, France

[2] Present address: Institute of Neuroscience - CNR & Humanitas Clinical and Research Center Via Manzoni 56, 20089 Rozzano (MI), Italy

[3] Institut Curie, PSL Research University, CurieCore Tech Mass Spectrometry Proteomics, 75005 Paris, France

[#] Correspondence: cecile.charrier@bio.ens.psl.eu

ABSTRACT

Human-specific genes are potential drivers of brain evolution. Among them, SRGAP2C contributes to distinct features by extending the period of synaptic maturation and increasing cortical connectivity. Here we examined SRGAP2 protein-interaction network in developing synapses and identified catenin delta-2 (CTNND2) as a binding partner of human-specific SRGAP2C. CTNND2 is a cadherin-binding protein implicated in intellectual disability in the Cri-du-Chat syndrome, severe autism and epilepsy. Using sparse manipulations in upper layer cortical pyramidal neurons, we demonstrate that CTNND2 is an activity-limiting protein that coordinates synaptic excitation and inhibition and controls intrinsic excitability in juvenile mice. Later in adults, CTNND2 is required for long-term maintenance of dendritic spines. CTNND2 enrichment at excitatory synapses is enhanced by human-specific SRGAP2C. Thus, while loss of CTNND2 function accelerates synaptic development, causes overexcitation and homeostatic failure, its upregulation by SRGAP2C may contribute to synaptic neoteny in humans and protect against precocious synapse loss during aging.

INTRODUCTION

During human evolution, cortical pyramidal neurons have specialized to mature over longer time scales, establish a greater number of synaptic connections, and integrate more information[1–13]. These distinctive features contribute to typically human cognitive abilities. They reflect unique regulations of neuronal and synaptic development and imply strong evolutionary constraints on key aspects such as the coordination between excitation and inhibition (E/I coordination), the temporal control of synaptogenesis, and neuronal excitability, whose defects cause neurodevelopmental disorders[14–18]. Despite growing understanding of human uniqueness at the genomic level[19–22], the impact of genetic innovations on neuron and synapse cell biology remains largely unexplored. We have previously shown that the human-specific gene *SRGAP2C* (Slit-Robo Rho GTPAse-activating protein 2C), regulates synaptic development and cortical connectivity[23–26]. *SRGAP2C* is the product of large segmental duplications that occurred about 3.3-2.4 million years ago, at a time coinciding with the emergence of the genus *Homo*[27–30]. It encodes a truncated copy of the ancestral protein SRGAP2A, a postsynaptic protein highly conserved in mammals that promotes the maturation of excitatory and inhibitory synapses and limits their density[23,24]. In neurons, SRGAP2C inhibits SRGAP2A, which delays synaptic maturation and increases synaptic density[23,24,31], two features characterizing human cortical pyramidal neurons compared to mouse or monkey neurons[1,2,8,32]. Thus, *SRGAP2* duplications provide a starting point to identify molecular pathways operating at the synapse that are likely to be uniquely regulated in humans.

In the present study, we identify catenin delta-2 (CTNND2) as a major binding partner of SRGAP2 proteins during synapse maturation. CTNND2 belongs to the delta subfamily of the catenin superfamily and is a component of the cadherin-catenin adhesion complex. It corresponds to a 132 kDa protein containing a N-terminal coiled-coil domain, 10 armadillo repeats that mediate binding to cadherins, and a C-terminal sequence containing a PDZ binding motif. It expression is virtually restricted to the brain and peaks during postnatal development[33]. CTNND2 was first identified in a yeast-2-hybrid screen as a binding partner of presenilin-1[34], the most frequently mutated gene in familial Alzheimer's disease. *CTNND2* is implicated in the Cri-du-Chat syndrome, where its hemizygous loss causes intellectual disability (ID)[35]. Point mutations in *CTNND2* have also been implicated in severe forms of autism spectrum disorders (ASD)[36] and in epilepsy[37]. In mice, *ctnnd2* mutation impairs synaptic plasticity, memory and cortical function[38,39]. CTNND2 has been involved in the regulation of excitatory synapses and dendritic spines, the postsynaptic site of excitatory synapses in pyramidal neurons, but with contrasting results[36,39–43]. Using sparse in vivo manipulation of *ctnnd2* expression in layer 2/3 pyramidal neurons of the somatosensory cortex, high-resolution confocal microscopy, electrophysiological recordings and quantitative proteomics, we demonstrate that CTNND2 is a multifunction protein that operates at excitatory

synapses, at inhibitory synapses and in the control of neuronal intrinsic excitability. During postnatal development, loss of CTNND2 function in postsynaptic neurons disrupts a subset of inhibitory synapses, accelerates excitatory synaptic development, enhances excitatory synaptic transmission, and causes hyperexcitability. Later in adult mice, CTNND2 deficiency leads to a precocious loss of synapses. At the molecular level, CTNND2 interacts with the inhibitory postsynaptic organizer gephyrin and is required for the synaptic recruitment of synGAP1 in dendritic spines, where the two proteins form an activity-limiting complex. CTNND2 enrichment in dendritic spines is increased by the human-specific protein SRGAP2C, suggesting an enhancement of CTNND2 synaptic function during human evolution that contributes to delay the maturation of synapses and promotes their long-term maintenance.

RESULTS

Identification of CTNND2 as a binding partner of the human-specific protein SRGAP2C

To identify the protein interaction network of SRGAP2 during synaptic maturation, we performed a quantitative proteomic screen based on the co-immunoprecipitation of endogenous SRGAP2 in synaptic fractions from postnatal day (P)15 mouse brains and label-free liquid chromatography tandem mass spectrometry (LC–MS/MS*)* (**Fig. 1a**). We identified CTNND2 among the 10% most enriched proteins in SRGAP2 complexes, among known direct partners such as SRGAP3, SRGAP1 and HOMER1[23,44] (**Fig. 1b**). SYNGO analysis (using SYNaptic Gene Ontologies database[45]) highlighted a strong implication of SRGAP2 interaction network in synapse organization (**Fig. 1c**)*.* Major partners participated in postsynaptic scaffolds and trans-synaptic adhesion, and CTNND2 surpassed all of them in terms of enrichment and abundance, as estimated by comparing the number of peptides obtained by proteomics per 100 kDa (**Fig. 1d**). Strikingly, co-immunoprecipitation in heterologous HEK cells revealed that CTNND2 directly interacts not only with ancestral SRGAP2A (ortholog of mouse SRGAP2) but also with SRGAP2C, a human-specific truncated copy of the ancestral protein (**Fig. 1e-f**). The strong implication of CTNND2 in neurological disorders[36,37,46] combined with its interaction with a family of proteins linked to human evolution protein suggested its importance in human brain development and function.

CTNND2 is required for inhibitory synapse formation but limits spine density in juvenile mice

To characterize CTNND2 function, we first examined its subcellular distribution using immunocytochemistry in dissociated cortical neurons cultured for 18 days in vitro (DIV). Endogenous CTNND2 formed clusters associated with the vast majority of both excitatory

synapses and inhibitory synapses, labelled with their respective core scaffolding proteins PSD-95 and gephyrin (PSD-95: 79% ± 4%, gephyrin: 67% ± 3%, Fig. 2a-b). This dual localization is atypical because excitatory and inhibitory synapses are built of almost distinct sets of proteins[47–49]. It suggested a potential role for CTNND2 in E/I coordination.

To test this hypothesis, we designed and validated shRNAs directed against *ctnnd2* (shCtnnd2, **supplementary fig. 1**), and we sparsely knocked it down in layer 2/3 pyramidal neurons (CPNs) of the somatosensory cortex using in utero electroporation (IUE) at embryonic days (E) 14.5 – 15.5 (**Fig. 2c**). We first examined the consequences on dendritic spines, as a proxy for excitatory synapses, by co-expressing the shRNAs with the fluorescent protein mVenus. We quantified spine density in oblique apical dendrites using high-resolution confocal microscopy. In juvenile mice (postnatal day (P) 21), CTNND2-depleted neurons exhibited a higher density of dendritic spines than neurons expressing a control shRNA (115% ± 4% of shControl; **Fig. 2d-e**). Normal spine density was rescued by co-electroporating shCtnnd2 with an shRNA-resistant *ctnnd2* variant (96 ± 4% of control, see also **supplementary fig. 1**). Sparse *ctnnd2* knockout using Crispr-Cas9 also increased spine density (115% ± 6% of Control; **supplementary fig. 2**). On the other hand, CTNND2 overexpression strongly reduced spine density (59 ± 4% of control; **Fig. 2 d-e**), highlighting the importance of CTNND2 dosage in spine development. We then examined the consequences of CTNND2 depletion on inhibitory synapses. To that aim, we in utero electroporated soluble tdTomato with low amount of EGFP-tagged gephyrin, which reliably labels inhibitory synapses without impairing their development[23,50–52]. C*tnnd2* depletion decreased the density of gephyrin clusters (79 ± 3% of control, **Fig. 2f-g**), which was rescued by co-expressing the shRNA-resistant construct (98 ± 4% of control). CTNND2 overexpression did not significantly increase gephyrin cluster density, although a trend was observed (105 ± 4%; **Fig. 2f-g**). Therefore, CTNND2 has opposite function at excitatory and inhibitory synapses: it is necessary for the formation and maintenance of some inhibitory synapses while it limits spine density.

Loss of CTNND2 increases the E/I ratio and intrinsic excitability in juvenile mice.

To assess the physiological consequences of CTNND2 inactivation, we performed whole-cell patch-clamp recording in acute brain slices (P16-P20) and compared synaptic transmission in electroporated CTNND2-depleted neurons versus neighboring non-electroporated control neurons (**Fig. 3a**). We first examined miniature excitatory and inhibitory postsynaptic currents (mEPSCs and mIPSCs, respectively). Loss of CTNND2 strongly increased the frequency of mEPSCs (140% ± 12% of control) without modifying their amplitude (108% ± 6% of control, **Fig. 3b-d**). By contrast, mIPSC amplitude and frequency were not affected by *ctnnd2* knockdown (115 ± 12% and 102 ± 11% of control respectively, **Fig. 3e-f**). Since whole-cell

patch clamp recordings mainly sample proximal synapses, these results combined with the loss of gephyrin clusters in oblique apical dendrites of ctnnd2-knocked-down neurons suggest that CTNND2 function in inhibition might be restricted to specific types of distal inhibitory synapses.

We then measured the ratio between excitatory and inhibitory transmission (E/I ratio) in oblique apical dendrites. To that aim, we placed a stimulation electrode ~100 μm along the main apical dendrite (**Fig. 3g**) and adjusted the stimulation strength to evoke a response of approximately 150 pA. Evoked excitatory and inhibitory postsynaptic currents (eEPSC and eIPSC) were recorded by clamping the cell at -70 mV and +10 mV, respectively (**Fig. 3h**). CTNND2 depletion strongly increased the E/I ratio compared to control neurons (185% of maximum current amplitude in control neurons and 152% of control synaptic charge over 50 ms, **Fig. 3i-j**). By contrast, the ratio between AMPA receptor- and NMDA receptor-mediated synaptic transmission was not affected by CTNND2 depletion in postsynaptic neurons (**supplementary fig. 3**).

Increases in E/I ratio might compensate or be compensated by a decrease in neuronal intrinsic excitability to preserve network activity[17]. To examine how CTNND2 deficiency affects intrinsic neuronal properties, we performed current-clamp recordings and measured changes in membrane potential and action potential firing in response to somatic current injections (**Fig. 4**). Although the resting membrane potential (Vrest) and spike threshold (Th) did not differ between control and CTNND2-deficient neurons ($Vrest_{Control}$ = -78 ± 1 mV, $Vrest_{shCtnnd2}$ = -76 ± 1 mV; $Th_{Control}$ = -37 ± 1 mV, $Th_{shCtnnd2}$ = -35 ± 1 mV), the membrane resistance of CTNND2-deficient neurons was higher (152 ± 11% of control), their input/output relationship stronger, their rheobase lower ($Rh_{Control}$ = 384 ± 23 pA, $Rh_{shCtnnd2}$ = 278 ± 20 pA) and they fired action potential at a much higher frequency than control neurons (162 ± 8% of control for 500 pA current injection). By contrast, no difference was observed when non-electroporated control neurons were compared to neurons electroporated with a control shRNA (**supplementary fig. 4**). Collectively, our results indicate that CTNND2 deficiency causes homeostatic failure in juvenile cortical pyramidal neurons, increasing the E/I ratio and ramping up intrinsic excitability.

Bi-phasic effect of CTNND2 deficiency

We next interrogated the time course of *ctnnd2* knockdown consequences by examining two other developmental time points: P10, which corresponds to an early time point during synaptogenesis, and P77, when mice have reached adulthood (**Fig. 5**). In control neurons, the density of dendritic spines strongly increased between P10 and P21 (from 0.49 ± 0.03 to 1.69 ± 0.04 spine.μm^{-1}) and then remained stable in adults (1.68 ± 0.08 spine.μm^{-1}, Fig. 5a-

b). In CTNND2-deficient neurons, spine density was not significantly different from control at P10 (0.53 ± 0.03 spine.μm^{-1}) but its rise between P10 and P21 was steeper than in control neurons, resulting in higher spine density at P21 (see also **Fig. 2**). Furthermore, the developmental increase in mEPSC frequency occurred earlier in CTNND2-deficient neurons and was more intense than in control neurons, with major differences between shCtnnd2 and control neurons around P11 (**Fig. 5c-g**), indicating that CTNND2 deficiency accelerates synaptic development. In adult mice however, spine density in CTNND2-deficient neurons was lower than in control neurons (82% ± 4% of control, **Fig. 5a-b**), consistent with previous work in a mouse model expressing a truncated mutant of CTNND2 loss of function[39]. Thus, *ctnnd2* deficiency has a biphasic effect, leading to early hyperexcitation followed by premature loss of synapses (**Fig. 5h**). To assess if spine loss could be prevented by bypassing the period of hyperexcitation, we used a conditional knockdown system (**Fig. 5i-j**). Expression of shCtnnd2 or shControl was induced after tamoxifen administration between P28 and P31 and spine density was quantified in P77 mice. Interestingly, this did not protect against spine loss in adult mice, indicating that CTNND2 is required for the long-term maintenance of synaptic structures independently of its function in synaptic development.

CTNND2 synaptic interactome

To understand how CTNND2 operates during synaptic development, we performed a quantitative proteomic screen and identified CTNND2 protein interaction network (**Fig. 6a-b**). SYNGO analysis of the most enriched partners highlighted their implication in synapse organization and assembly, trans-synaptic interactions, chemical synaptic transmission, regulation of neurotransmitter receptor level at synapses and regulation of plasma membrane potentials, consistent with our morphological and physiological results (**Fig. 6c**). More specifically, members of the cadherin/catenin superfamily were highly represented among the main partners of CTNND2 (**Fig. 6b,d**), and other proteins involved in cell-cell interactions were detected too, indicating widespread implication of CTNND2 at cell-cell contacts (**Fig. 6d**). In agreement with the role of CTNND2 in neuronal excitability, CTNND2 partners included potassium/sodium hyperpolarization-activated cyclic nucleotide-gated channels (HCN1-4), their accessory subunit Pex5l[53,54], and potassium channels KCND2 (Kv4.2) and KCNH3[55,56]. However, the two most striking partners of CTNND2 were the excitatory postsynaptic protein SynGAP1 and the inhibitory postsynaptic organizer gephyrin, which were among the most represented proteins (>90 peptides per 100 kDa) in CTNND2 protein complexes (**Fig. 6b,d**). Glutamatergic AMPA, NMDA and metabotropic receptor subunits, as well as GABAergic (Gagrb2) neurotransmitter receptor subunits were also found in complex with CTNND2 (**Fig. 6d**), although with less peptides relative to their molecular weight, further supporting the dual role of CTNND2 at excitatory and inhibitory synapses.

SynGAP1 is one of the most abundant proteins of excitatory postsynaptic densities (PSDs)[48]. Its haploinsufficiency accounts for up to 1% of non-syndromic ID in humans[57] and, like CTNND2 deficiency, it accelerates excitatory synaptic maturation in mice[58]. To tackle a possible interplay between CTNND2 and SynGAP1, we co-electroporated in utero SynGAP1-GFP along with tdTomato and either shCtnnd2 or shControl, and we analyzed SynGAP1 accumulation in dendritic spines along oblique apical dendrites of layer 2/3 CPNs at P21. CTNND2 deficiency led to a dramatic loss of SynGAP1 in spines (44 ± 9% of control, **Fig. 6e**), without changes in the level of PSD-95 labelled with GFP-tagged FingRs[59] (level: 113 ± 24% of control, **Fig. 6f**), demonstrating that CTNND2 is necessary for the synaptic accumulation of SynGAP1. Last, we interrogated the functional relevance of CTNND2 interaction with SRGAP2 (**Fig. 1**) by testing if and how the human-specific protein SRGAP2C regulates CTNND2 subcellular distribution. In agreement with our previous work[23,24], juvenile mouse layer 2/3 CPNs expressing SRGAP2C exhibited lower levels of PSD-95 in dendritic spines (75 ± 5% of control), reflecting a delay in synapse assembly. By contrast, SRGAP2C expression enhanced the enrichment of CTNND2-GFP in spines (146 ± 8% of control, **Fig. 6g-h**), suggesting a strengthening of CTNND2 synaptic function. Collectively, these data provide important insights into the role of CTNND2 as an activity-limiting factor and its regulation by a human-specific protein.

DISCUSSION

The cellular and molecular bases underlying human-specific traits of brain development and function are a central question in neuroscience, evolution and medicine. By investigating the protein-protein interaction network of SRGAP2, one of the few genes specifically duplicated in humans and the only one involved in synapses so far, we identified CTNND2 at the crossroad of human evolution and neurological disorders and we characterized its function at synapses in pyramidal neurons of the neocortex. Our results demonstrate a pivotal role of CTNND2 in coordinating synaptic excitation and inhibition, controlling intrinsic excitability, setting the pace of synaptic maturation and supporting the maintenance of synaptic structures during adulthood. CTNND2 loss of function has deleterious consequences that reflect a failure of neuronal homeostasis[16,17] and are compatible with the neurological disorders in which it is implicated[37,39,46]. By contrast, CTNND2 enrichment at synapses is enhanced by the human-specific protein SRGAP2C. Thus, CTNND2 regulation by SRGAP2C likely contributes to prolong the period of synaptic development in human neurons and protect against spine loss during ageing.

Although CTNND2 implication in cognition and brain disorders is well established[36,38,39,46], its role at synapses has remained debated. Some studies suggested its

requirement for spine formation, but others concluded that CTNND2 limits synapse density or that it is only required later in adults (e.g.[36,39–42], but see[43]). The reasons of these discrepancies are unclear but they possibly reflect differences between the models that were used (cortex versus hippocampus, in vitro versus in vivo, young versus adult neurons, or the use of a mutant mouse model that still expresses the first 447 amino-acids of CTNND2[38], a portion containing most of the mutations identified in severe autism[36]). Using a sparse knockdown and knockout strategy and analysis at key developmental time points, our results uncover the versatility of CTNND2 function as an activity-limiting protein during postnatal development and a protein required for spine maintenance in adults. In young and juvenile CTNND2-deficient neurons, the acceleration of synaptic maturation, the global excess of excitation and excitability, and changes in synaptic connections are likely to impact the organization of cortical circuits and critical periods of plasticity[16,17,60], which might account for neurodevelopmental disorders in patients with CTNND2 mutations[36,37,46]. In adults, the premature loss of synapses we observe in CTNND2-deficient neurons in vivo is consistent with the progressive retraction of dendrites and dendritic spines in mice carrying a CTNND2 truncation[39]. The parallel between the cellular phenotypes observed in adult mice following sparse *ctnnd2* knockdown (here) and global *ctnnd2* truncation[39] indicate that CTNND2 function in the cortex is mostly postsynaptic and cell autonomous. In *ctnnd2* mutant mice, these changes are associated with deficits in cortical responsiveness and cognition[38,39] and might be signs of neurodegeneration. This hypothesis is supported by evidence that presenilin1 mutations implicated in familial Alzheimer's disease increase the processing of CTNND2[34,39,46,61]. Remarkably, we find that preserving *ctnnd2* expression during neuronal and synaptic development using a controlled knockdown system is not sufficient to ensure the long-term maintenance of synaptic and neuronal structures, showing that spine loss in adult neurons does not result from developmental excitotoxicity.

Our proteomic analysis identifies Gephyrin as one of the most prominent partners of CTNND2. Taking into account the high level of association between gephyrin clusters and CTNND2 in cortical neurons, and the loss of inhibitory synapses in the oblique apical dendrites of CTNND2-deficient neurons, we postulate that CTNND2 links trans-synaptic adhesion systems to the inhibitory postsynaptic scaffold to ensure proper inhibitory synapse formation and maintenance. Future experiments will determine which inhibitory circuits are regulated by CTNND2 and whether CTNND2 function in inhibition is regulated by SRGAP2C. Another major partner of CTNND2 we identified in maturing synapses is SynGAP1, a protein virtually as abundant as PSD-95 in excitatory PSDs[48]. Like CTNND2, Syngap1 is implicated in ID, autism and epilepsy and like CTNND2, it is an activity-limiting protein[15,57]. In the cortex, SynGAP1 and CTNND2 deficiency have similar outcomes[62], leading to biphasic perturbations with early hyperexcitation and faster synaptogenesis followed by adult hypofunction[15,63]. We establish that CTNND2 is required for the synaptic recruitment of SynGAP1. This supports a

model in which CTNND2 and SynGAP1 form a core protein complex that shapes the developmental trajectory of synapses. This also suggests shared synaptic pathophysiology in neurological disorders linked to loss-of-function mutations in their genes. Furthermore, we find that CTNND2 enrichment in dendritic spines is enhanced in SRGAP2C-expressing neurons, despite decreased synaptic levels of PSD-95. Interestingly, CTNND2 accumulation in excitatory PSDs has been shown by others to be regulated by Shank3[64], a prototypical postsynaptic scaffolding protein associated with Phelan-McDermid syndrome and idiopathic autism[15] whose mutations in mice also induce a wide array of defects[15,63]. Together, these data raise important questions on the hinge between the assembly of the postsynaptic scaffold and the recruitment of activity-limiting proteins to precisely tune synaptic activity during development.

In the human neocortex, synaptic development is extremely protracted but the metronome remains poorly understood. We have previously shown that the human-specific protein SRGAP2C regulates the timing of synaptic development, in part by regulating its parental copy SRGAP2A and decelerating the assembly of the Homer-based excitatory postsynaptic scaffold[23]. The interaction between SRGAP2C and the activity-limiting protein CTNND2 opens new perspective to understand how synaptic development is adjusted in humans at the core of postsynaptic scaffolds. It also raises the hypothesis that the disruption of synaptic regulations specific to humans contributes to the pathogenesis of neurological disorders.

ACKNOWLEDGMENTS

We thank all the members of the Charrier lab for helpful discussion. We thank, D. Arnold, B. Rico, C. Cepko, F. Polleux, F. Zhang, X. Morin and W.L. Jin for sharing reagents. This work was supported by INSERM, CNRS, ENS, the Agence Nationale de la Recherche (ANR-13-PDOC-0003 and ANR-17-ERC3-0009 to C.C.), the European Research Council (ERC starting grant 803704 to C.C.), Labex Memolife, Fondation pour la Recherche Médicale (to N.M.A and D.L.) and Région Ile-de-France (to D.L.).

COMPETING INTERESTS

The authors declare no competing interests.

AUTHOR CONTRIBUTIONS

N.A., M.D and M.F performed experiments. N.A., M.D, M.F. and C.C analyzed data and interpreted the results. F.D. carried out the MS experimental work, D.L. supervised MS and data analysis. N.A and C.C. designed the study, prepared the figures, and wrote the manuscript. C.C. supervised the project and provided funding.

METHODS

Animals

All animals were handled according to French and EU regulations (directive 2010/63, decree 2013-118). Authorization references were #1530-2015082611508691v3 and #29476 2021020311595454v5, delivered by the French Ministry of Research after evaluation by the Comité d'Ethique en Experimentation Animale n°005. In utero electroporations were performed on pregnant Swiss females at E14.5-15.5 (Janvier labs) and electroporated offspring was used for experiments at varying postnatal timepoints (P10, P15-23 and P77) without consideration for their sex. Primary cultures were prepared from timed pregnant C57BL/6J or Swiss mice at E17.5-E18.5 (Janvier labs). Mice were maintained in a 12 hours light/dark cycle with unlimited access to food and water.

Primary neuronal cultures

Primary cultures of cortical neurons were performed as previously described[23] with few modifications. Briefly, mouse cortices from E18.5 embryos were dissected, dissociated and neurons were plated on glass coverslips coated with poly-D-ornytine (80 μg/ml, Sigma) in MEM (Gibco) supplemented with sodium pyruvate, L-glutamine (2 mM) and 10% horse serum. This medium was exchanged 2-3 hours after plating with Neurobasal (Gibco) supplemented with L-glutamine (2 mM), B27 (1X) and penicillin (2.5 units/ml) - streptomycin (2.5 mg/ml). Until use, every 5 days one third of the medium was changed and the cells were maintained at 37°C and 5% CO2. Unless otherwise indicated, all products were from Thermo Fisher Scientific.

Cell lines

HEK293T (CRL-1573 from ATCC) cells were cultured according to suggested protocols. Cells were maintained in DMEM (GIBCO) supplemented with 10% fetal bovine serum (GIBCO) and 1% Penicillin-Streptomycin (GIBCO) at 37°C, 5% CO2. They were passaged by trypsin/EDTA digestion (GIBCO) upon reaching confluency with a maximum of 25 passages.

Plasmids for protein expression

All plasmids for protein expression *in utero* have a pCAG backbone driving protein expression under the CAG promotor. pCAG EGFP-GPHN was previously described[23] and was used to visualize inhibitory synapses. pCAG SRGAP2A-HA and pCAG SRGAP2C-HA were previously described[23,24]. For pCAG CTNND2-EGFP, human CTNND2 cDNA was obtained from Horizon (Clone IMAGE 40080647; Insert sequence: BC111837) subcloned by PCR and inserted in pCAG between HindIII and AgeI; pCAG CTNND2-Myc was created through digestion of pCAG CTNND2-EGFP between Age1 and NotI to remove the GFP and insertion of the DNA cassette containing 3xMYC with compatible ends; For rescue experiments, four silent point mutations were introduced in *ctnnd2* (c3242a_a3243t_g3244c_c3245t) to resist to shRNA-mediated knockdown (mutant named *ctnnd2**). For pCAG SYNGAP-EGFP, SYNGAP1 was amplified from cDNA (Horizon; ORFeome Collab. Hs SYNGAP1 ORF w/o Stop Codon; Clone IMAGE: 100015293; insert sequence: BC148357) and inserted into pCAG between BsrGI and NotI. pCAG_GPHN.FingR-eGFP-CCR5TC was a gift from Don Arnold (Addgene plasmid #46296 ; http://n2t.net/addgene:46296 ; RRID:Addgene_46296[59]).

shRNA plasmids and Crispr-Cas9 plasmids

To express shRNAs, we used the previously described pH1SCV2 and pH1SCTdT2 vectors[23,24] in which the H1 promoter drives the expression of the shRNA and a CAG promoter that of either mVenus (pH1SCV2) or TdTomato (pH1SCTdT2). mVenus was used for dendritic spine analysis. pH1SCTdT2 was used in patch clamp experiments, and along with pCAG EGFP-GPHN in morphology experiments to analyze inhibitory synapse densities. The control shRNA (shControl) was described previously[24]. To target *ctnnd2* we inserted the following seed sequences into the shRNA vectors: shCtnnd2#1 5'- GCAGTGAGATCGATAGCAAGA -3' and shCtnnd2#2 5'-GGGAAATGATCAGCCTCAAAG -3'. Both shRNAs were used in spine density analysis at P21 and no difference was observed between the them. In all the other experiments, we used shCtnnd2#2. The mutant *ctnnd2** is resistant against shCtnnd2#2. If not otherwise indicated shCtnnd2#2 was used in experiments. For conditional knock-down experiments, shControl or shCtnnd2 were inserted into pCAG-mir30 (Addgene plasmid #14758[65]) between EcoRI and XhoI. Then, the miR-30a-shRNA cassette was then amplified and inserted into pDIO-DSE-mCherry-PSE-MCS (gift from Beatriz Rico (Addgene plasmid #129669 ; http://n2t.net/addgene:129669 ; RRID:Addgene_129669[66]) between PmeI and EcoRV. For Crispr-Cas9 knockout experiments, gRNAs were designed using the prediction software. https://portals.broadinstitute.org/gpp/public/analysis-tools/sgrna-design and inserted in pX330-U6-Chimeric_BB-Cbh-hSpCas9 (gift from Feng Zhang (Addgene plasmid #42230 ; http://n2t.net/addgene:42230 ; RRID:Addgene_42230[67]). The sequence of the gRNA targeting *ctnnd2* was GGAGCGATGCAAGCTTGGCT (in exon 3).

Lentiviral plasmids and lentivirus production

To knockdown mouse *ctnnd2* with lentivirus, we used a lentiviral vector expressing shRNAs under a H1 promoter and GFP under a synapsin promoter, as previously described[68]. For production, HEK293T cells were co-transfected with the lentiviral vector expressing the shRNAs and three plasmids together comprising the lentiviral packaging system. 48h after transfection, the viral supernatant was collected and ultracentrifuged at 4°C at 25,000 g for 2h. Viral pellets were resuspended in sterile PBS, aliquoted and stored at -80°C.

shRNA validation

shRNAs were validated in HEK293T cells on exogenously expressed CTNND2 and on endogenous CTNND2 in primary cultures of cortical neurons. Briefly, for validation in a heterologous system, HEK293T cells were co-transfected using Jet-Prime (Polyplus Transfection #POL114-07) according to the manufacturer protocol with either MYC tagged CTNND2 or CTNND2* together with the shRNAs targeting CTNND2 or a control shRNA at a 1:2 ratio. Two days after transfection, cells were collected and lysed in RIPA buffer (150 mM NaCl, 1.0% NP-40, 0.5% sodium deoxycholate, 0.1% SDS, 50 mM Tris, pH 8.0, Sigma-Aldrich) and further processed for western blot analysis of the relative protein expression levels. Conditional knockdown validation was performed in HEK cells by co-expressing pDIO-DSE-mCherry-PSE-MCS containing our shRNAs and pCAG Cre. For the knockdown validation on endogenous *ctnnd2*, primary cultures of cortical neurons were infected at 4 days in vitro (DIV4) with lentiviruses carrying shCtnnd2#2 or a control shRNA. Infected cultures as well as a non-infected control were harvested at DIV21 and lysed in RIPA buffer under agitation for 1h at 4°C and further processed for western blot analysis (see below).

In utero electroporation

In utero electroporation (IUE) was performed as previously described[23,69]. Pregnant Swiss females at E14.5-15.5 (Janvier labs) were anesthetized with isoflurane (3.5% for induction and 1.5-2.5% during the surgery; ISO-VET Piramal Critical Care) and subcutaneously injected with 0.1 mg/kg of buprenorphine for analgesia. The uterine horns were exposed after laparotomy to enable injection of endotoxin-free DNA mix into one ventricle of the mouse embryos. The injected embryos were then electroporated with 4 pulses of 40 V for 50 ms at 500 ms intervals delivered by tweezer-type platinum disc electrodes (5 mm-diameter, Sonidel) and a square wave electroporator (ECM 830, BTX). The volume of injected DNA mix was adjusted depending on the experiments. Plasmids were used at the following concentrations: shRNA vectors: 0.5 μg/μl (adults) or 1 μg/μl (young animals; P10-P23); CTNND2 or shRNA-resistant

CTNND2*: 1 μg/μl; EGFP-GPHN: 0.3 μg/μl, SYNGAP-EGFP, SRGAP2C-HA and PSD-95-FingR GFP: 0.7 μg/μl. For conditional knockdown experiments, pCAG-EGFP was co-expressed with pCAG-ERT2CreERT2 and pDIO-DSE-mCherry-PSE-MCS containing our shRNAs (0.5 μg/μl each). For Crispr-Cqs9 knockout experiments, pX330-U6-Chimeric_BB-Cbh-hSpCas9 containing gRNA (0.5 μg/μl) was co-expressed with pCAG-EGFP (1 μg/μl).

Confocal imaging

Immunocytochemistry

After 18 days in vitro (DIV), cultured cortical neurons were fixed for 15 min at room temperature using 4% (w/v) paraformaldehyde in PBS and incubated for 30 min in blocking buffer containing 0.3% Triton X100 and 3% BSA (Sigma) in PBS to permeabilize the cells and block nonspecific staining. Subsequently, cells were incubated for 1h in primary antibody, rinsed extensively, and incubated 45 min in secondary antibodies diluted in blocking buffer. Coverslips were mounted on slides with Vectashield (Vector Laboratories). Primary antibodies were mouse anti-Gephyrin. (mAb7a, Synaptic System, 1:300), mouse anti-PSD-95 (clone K28/43, Neuromab, 1:200) and rabbit anti-CTNND2 (Abcam #ab184917; 1:500). Secondary antibodies were anti-rabbit Alexa-488 (Invitrogen; 1:500) and anti-mouse Cy3 (Jackson ImmunoResearch, 1:500).

Perfusion and slice preparation

Electroporated mice were sacrificed at the indicated age by terminal transcardial perfusion of 4% paraformaldehyde (Electron Microscopy Sciences) in PBS as described previously[68]. Unless otherwise indicated, 100 μm coronal brain sections were obtained using a vibrating microtome (Leica VT1200S, Leica Micro- systems). Sections were mounted on slides in Vectashield.

Confocal image acquisition

Confocal images were acquired in 1024x1024 mode using either Leica TCS SP8 scanning confocal microscope controlled by the LAFAS software and equipped with a tunable white laser and hybrid detectors (Leica Microsystems) or Nikon A1R HD25 scanning confocal microscope controlled by NIS Elements and equipped with an LU-N4/N4S 4-laser unit including 405 nm, 488 nm, 561 nm and 640 nm lasers. On the Leica TCS SP8, we used a 10X PlanApo objective (NA 0.45) to identify electroporated neurons and acquire low magnification images and a 100X HC-PL APO, NA 1.44 CORR CS objective to acquire higher magnification images and z-stacks of dendrites. On the Nikon microscope, we used the following objectives: Plan Apo Lambda 10x Air NA 0.45 (MRD00105) and SR HP Plan Apo Lambda S 100x Silicone

NA 1.35 (MRD73950). Z-stacks were acquired with 150 nm spacing and a zoom of x 1.24. Images were blindly acquired and analyzed.

Confocal image analysis

In immunocytochemistry experiments, the association of CTNND2 with Gephyrin or PSD-95 was analyzed using ICY v1.9.9.1[70]. Regions of interest were manually drawn around dendrites and clusters in each channel were detected using the spot detector plugin[71] of ICY. Then the association between channels was assessed with SODA 2-channel colocalization protocol[72] using the synaptic markers as reference channel (radius set to 1.5x the max. feret diameter). The fraction of gephyrin and PSD-95 clusters associated with a cluster of CTNND2 was defined as association index.

In brain slices, dendritic spines and Gephyrin cluster densities were quantified in oblique dendrites originating from the apical trunk using Fiji[73] (https://fiji.sc/). Only dendrites that were largely parallel to the plane of the slice and acquired from sections of comparable rostro-caudal position were analyzed (no more than 1 dendrite per neuron). The density of dendritic spines and gephyrin clusters along dendrites was calculated as described before[23,24]. Gephyrin cluster and spine densities were quantified over a minimal dendritic length of 50 μm starting from the object closest to the branchpoint with the main apical dendrite. The length of the dendritic segment was measured on the z projection. For conditional knockdown experiments, only cells expressing EGFP and mCherry, whose expression was induced by recombination after tamoxifen exposure were analyzed and spines were quantified based on EGFP fluorescence. To SynGAP1 and PSD-95 levels in spines, ROIs were manually drawn around dendrites and clusters were detected using the ICY spot detector plugin. Fluorescence intensity associated with SynGAP1 and PSD-95 in each spine was normalized to mean local filler intensity and compared between conditions. Since CTNND2-GFP signals were located at the periphery of the spines and CTNND2 was also diffuse in the shaft, fluorescence intensity associated with CTNND2 in spines was normalized to CTNND2 fluorescence in the dendritic shaft. All images were blindly analyzed.

Ex vivo electrophysiology

Slice preparation

Following in utero electroporation, juvenile (postnatal day 16-20) swiss mice were anesthetized with isoflurane (ISO-VET, Piramal Critical Care), decapitated and brains were quickly removed. For Inhibitory and excitatory miniature post-synaptic miniature currents (mIPSCs and mEPSCs, respectively) and intrinsic excitability recordings brains were subsequently placed in ice-cold (4°C) cutting solution containing (in mM): 85 NaCl, 64 sucrose,

25 glucose, 2.5 KCl, 1.2 NaH_2PO_4, 24 $NaHCO_3$, 0.5 $CaCl_2$, and 7 $MgCl_2$, saturated with 95% O_2 and 5% CO_2 (pH 7.3–7.4). Acute coronal slices were cut using the 7000 smz-2 vibratome (Campden Instrument). Slices recovered at room temperature in oxygenated artificial cerebrospinal fluid (ACSF) containing (in mM): 125 NaCl, 2.5 KCl, 2 $CaCl_2$, 1 $MgCl_2$, 1.2 NaH_2PO_4, 24 $NaHCO_3$, and 25 glucose (pH 7.4) for at least 45 min. For electrophysiological recordings, slices were transferred to a submerged recording chamber and continuously perfused at 33–34°C with oxygenated ACSF at a rate of 4 ml/min.

For E/I and AMPA/NMDA ratio as well as paired pulse ratio recordings the cutting solution contained (in mM): 83 NaCl, 2.5 KCl, 3.3 $MgSO_4$, 1 NaH_2PO_4, 22 Glucose, 72 Sucrose, 0.5 CaCl and the extracellular solution contained (in mM): 119 NaCl, 2.5 KCl, 1.3 $MgSO_4$, 1.3 NaH_2PO_4, 20 Glucose, 26 $NaHCO_3$, 2.5 CaCl.

Electrophysiological recordings

Whole-cell voltage or current clamp recordings were acquired from visually identified electroporated or non-electroporated layer 2/3 cortical pyramidal neurons of the somatosensory cortex. For all electrophysiological experiments an IR-DIC microscope (Olympus) was used, equipped with a 4X objective (UPlanFL, NA 0.13) as well as a 40X water immersion objective (LUMPlan Fl/IR, NA 0.8), 2 automated manipulators (Patchstar, Scientifica) and a ORCAFlash 4.0LT camera (Hamamatsu). Signals were recorded with a Multiclamp 700B Amplifier (Axon instruments), Axon Digidata 1550 (Axon Instruments) and pClamp 10 software (Axon instruments). Borosilicate glass pipettes were pulled to have a resistance of 3-7 MΩ. mIPSCs and mEPSCs were recorded at a holding potential of -60 mV in the presence of 0.5 μM TTX. mIPSCs were isolated by adding NBQX (10 μM) and D-AP5 (50 μM) to the ACSF and by using a high chloride intracellular solution containing (in mM): 150 KCl, 1.5 $MgCl_2$, 10 HEPES, 1 EGTA, 2 NaATP, 0.5 NaGTP (pH adjusted to ±7.3 with KOH). mEPSCs were isolated using gabazine (10 mM). For mEPSCs recordings as well as intrinsic excitability recordings the following intracellular solution was used, containing (in mM): 144 K-gluconate, 7 KCl, 10 HEPES, 1 EGTA, 1.5 $MgCl_2$, 2 NaATP, 0.5 NaGTP, (pH adjusted to ±7.3 with KOH). To record intrinsic excitability cells were held in current clamp mode at resting potential and injected with 1s step currents from -100 pA to +1000 pA with 50 pA increments to assess spike frequency. Current ramps from 0-1000 pA over 1s were used to probe the action potential threshold. E/I ratio, PPR ratio and AMPA/NMDA ratio were recorded with the following intracellular solution (in mM; previously described in Adesnik & Scanziani, 2010): 115 $CsMeSO_3$, 8 NaCl, 10 HEPES, 0.3 NaGTP, 4 MgATP, 0.3 EGTA, 5 QX-314, 10 BAPTA (pH adjusted to ±7.3). For all three types of recordings a stimulation electrode was placed approximately 100 μm up the apical dendrite and synaptic transmission evoked at 10

s intervals. For the E/I ratio and PPR recordings the neuron was clamped at -70 mV, the reversal potential of inhibitory synaptic transmission, and subsequently at +10 mV, the reversal potential of excitatory synaptic, to record 10 sweeps of eEPSCs and eIPSCs, respectively. Reversal potentials were validated in a few cells with 10 μM NBQX and 10 μM Gabazine respectively. The E/I ratio was calculated from the average peak currents or integrated currents (charge) per holding potential. For the paired pulse ratio, peak currents at both holding potentials were recorded in response to two sequential stimulations with a 50 ms interval (10 sweeps). The AMPA/NMDA ratio was recorded in the presence of 10 mM Gabazine and is defined as the peak of the EPSC at -70 mV over the amplitude of the EPSC at +40 mV 50 ms after stimulation (5 sweeps per holding potential). In all recordings, access and input resistance were monitored by applying 5 mV hyperpolarizing steps of current. All toxins were obtained from Abcam, salts and other reagents from Sigma Aldrich if not otherwise indicated.

Electrophysiological data analysis

Voltage and Current clamp data were sampled at 10 kHz and filtered at 2 kHz. All traces were analyzed using pClamp 10.0 (Molecular Devices). Miniature currents were analyzed over 1 min-periods. Overlapping events were excluded from amplitude analysis. Evoked currents were averaged over 10 (E/I ratio and PPR) or 5 sweeps (A/N ratio) and quantified over 50 or 100 ms after stimulation, respectively. Sweeps with a di-synaptic response or noise interference were excluded from averaging. The E/I ratio was calculated from either the maximum amplitude or integrated currents over 50ms (charge) per holding potential. The paired pulse ratio was calculated from the maximum amplitude of currents per holding potential. The AMPA/NMDA ratio is defined as the peak of the EPSC at -70 mV over the amplitude of the EPSC at +40 mV 50 ms after stimulation. Cells showing >20% change in access and input resistance upon application of 5 mV hyperpolarizing steps of current were excluded from the analysis.

Biochemistry experiments

Co-Immunoprecipitation in HEK cells

Transfected HEK cell were lysed in 10 mM Tris/Cl pH7.5, 150 mM NaCl, 0.5 mM EDTA and 0.5% Igepal and the protein concentration was determined. From each condition, 0.8-1 mg of total protein was diluted in binding buffer containing 0.05% Igepal, 10 mM Tris/Cl (pH 7.5), 150 mM NaCl, 0.5 mM EDTA and protease inhibitors as well as 25 μl of antibody-conjugated magnetic beads. Depending on the experiment GFP-, MYC- or HA-conjugated magnetic beads were used (GFP-trap and MYC-trap from Chromotek or Pierce anti-HA magnetic beads

(Thermo Fisher #88837) respectively). Samples were incubated with the beads for 2 hours at 4°C. After extensive washes, the beads were resuspended in Laemmli buffer and bound proteins were released by boiling (5 min 95°C). Samples were subjected to western blot analysis. Inputs correspond to 15 μg of proteins.

Western blotting

Western blotting was performed using precast gels, electrophoresis and transfer chambers from BioRAD according to standard procedures. The following primary antibodies were used: rabbit anti-HA (Cell Signalling #3724S, 1:1000), rabbit anti-GFP (Thermo Fisher Scientific #A11122, 1:2,000), mouse anti-Myc (Cell Signaling Technology #2276, 1:1,000), mouse anti-CTNND2 (Abcam #ab54578, 1:1000), rabbit anti-CTNND2 (Abcam #ab184917; 1:1000), and mouse anti-actin (Sigma Aldrich, #MAB1501R, 1:5000). Donkey anti-mouse or anti-rabbit HRP-conjugated secondary antibodies were used at a 1:10,000 dilution (Jackson Immunoresearch #711-035-150 and #711-035-152 respectively). Protein visualization was performed by chemiluminescence using LumiLight western blotting (Roche) and ImageQuant 800 (GE Healthcare).

Subcellular fractionation and co-immunoprecipitation

Subcellular fractionation was performed from Swiss P15 mouse brains as previously described [68]. All steps were performed at 4°C. Briefly, brains were homogenized in ice-cold HEPES-buffered sucrose (0.32 M sucrose, 4 mM HEPES pH 7.4, 5 mM EDTA, 5 mM EGTA, protease inhibitor cocktail, from Sigma) using a motor driven glass-teflon homogenizer. The homogenate was centrifuged at 3,000 g for 15min. The resulting supernatant was centrifuged at 38,400 g for 15 min, yielding the crude synaptosomal pellet. The pellet was then subjected to hypo-osmotic shock and centrifuged at 38,400 g for 20 min. The resulting pellet was lysed for 1 hour using HEPES-buffered NaCl (100 mM NaCl, 4mM HEPES pH 7.4, 5 mM EDTA, 5 mM EGTA, protease inhibitor cocktail) supplemented with 1% CHAPS (Sigma) and centrifuged at 100,000 g for 1 h. The corresponding supernatant is referred to as synaptic fraction or synaptic membranes. Protein concentration was measured using BCA assay (Pierce) and protein samples were subjected to immunoprecipitation. Co-immunoprecipitation were performed using antibodies covalently cross-linked to protein G magnetic beads (Pierce). 36 μg of rabbit anti-CTNND2 or anti-SRGAP2 (directed against the N-rerminal[23], gift from Franck Polleux and Wei Lin Jin) antibodies, or total rabbit IgG in control condition, were incubated for 1h at room temperature and cross-linked with 20 mM DMP (dimethylpimelimidate, Pierce) in 0.2 M Sodium Borate pH 9. After 30 min, the reaction was blocked for 1 hour with 0.2 M Ethanolamine (pH 8). Eventual unbound antibody molecules

were washed out by incubating the beads for 5 min in 0.1 M glycine (pH 3). The efficiency of cross-linking was checked by running samples on polyacrylamide 4%–15% gradient gels (Biorad) followed by Comassie Blue staining. 1 mg of total proteins from purified synaptic membranes were diluted in a HEPES-NaCl buffer containing (in mM): 20 HEPES pH 7.4, 150 NaCl, 5 EDTA, 5 EGTA and protease inhibitor cocktail supplemented with 1% CHAPS and incubated overnight at 4°C with antibody-coupled magnetic beads. The beads were rinsed 3 times using HEPES-NaCl buffer supplemented with 0.1% CHAPS and further washed 3 times in a buffer containing 20 mM HEPES (pH 7.4) and 150 mM NaCl. The samples were then subjected to mass spectrometry analysis (see below).

Mass spectrometry

Proteomics analysis was performed as previously described[68]. Proteins bound to magnetic beads were washed twice with 100 µL of 25 mM NH4HCO3 and on-beads digested with 200 ng of trypsine/LysC (Promega) for 1 hour in 100 µL of 25 mM NH4HCO3 at room temperature. The peptides were loaded onto an C18 StageTips[68] for desalting and eluted using 40/60 MeCN/H2O + 0.1% formic acid. Mass spectrometry measurement was performed on an Orbitrap Fusion Tribrid mass spectrometer (Thermo Scientific) coupled online to an RSLCnano system (Ultimate 3000, Thermo Scientific) and with a top speed DDA method using higher-energy C-trap collisional dissociation (HCD) fragmentation analyzed in the linear ion trap in rapid mode. The mass spectrometry proteomics data have been deposited to the ProteomeXchange Consortium via the PRIDE[75] partner repository with the dataset identifiers PXD036488 and PXD036487. For protein identification, data were searched against the Mus musculus (Mouse) UniProt database using Sequest^{HT} through proteome discoverer (version 2.1). Enzyme specificity was set to trypsin and a maximum of two missed cleavage site were allowed. Oxidized methionine, N-terminal acetylation, and carbamidomethyl cysteine were set as variable modifications. Maximum allowed mass deviation was set to 10 ppm for monoisotopic precursor ions and 0.6 Da for MS/MS peaks. The resulting files were further processed using myProMS[76] v3.9.3. FDR calculation used Percolator and was set to 1% at the peptide level for the whole study.

Proteomics analysis: label-free quantification

Label free quantification was performed by peptide Extracted Ion Chromatograms (XICs) computed with MassChroQ version 2.2.1[77]. For protein quantification, XICs from proteotypic and non-proteotypic peptides shared between compared conditions (TopN matching), and all charge states and sources were used. Global MAD or median and scale normalization was applied on the total signal to correct the XICs for each biological replicate (n=3). To estimate the significance of the change in protein abundance, a statistical test based on a linear model

adjusted on peptides and biological replicates was performed and *p*-values were adjusted with a Benjamini–Hochberg FDR procedure.

Gene ontology analysis

Gene ontology analysis was performed using the SYNGO database (https://syngoportal.org/)[45].

Statistical analysis

Statistical analyses were performed with Prism 7 (GraphPad Software). Data are obtained from a minimum of three independent experiments. For in utero electroporations data were obtained from at least three experiments or three animals from two independent litters. For statistical analysis, normality of the distributions was assessed using the D'Agostino-Pearson normality test. In case of normal distributions, we used paired or unpaired Student's t test or one-way analysis of variance followed by Tukey's post hoc test. Non-normal distributions were assessed using the non-parametric Mann-Whitney test, paired Wilcoxon test, or Kruskal-Wallis test followed by Dunn's multiple comparison test. In boxplots, whiskers correspond to the minimal and maximal values. Other data represent mean ± SEM. Sample size and statistical tests are reported in each main and supplementary figure. The significance threshold was placed at $p < 0.05$ (NS= $p > 0.05$; *= $p < 0.05$, **= $p <0.01$; ***= $p<0.001$).

REFERENCES

1. Benavides-Piccione, R., Ballesteros-Yanez, I., DeFelipe, J. & Yuste, R. Cortical area and species differences in dendritic spine morphology. *J Neurocytol* **31**, 337–346 (2002).
2. DeFelipe, J. The evolution of the brain, the human nature of cortical circuits, and intellectual creativity. *Front. Neuroanat.* **5**, (2011).
3. Szegedi, V. *et al.* Plasticity in Single Axon Glutamatergic Connection to GABAergic Interneurons Regulates Complex Events in the Human Neocortex. *PLoS Biol* **14**, e2000237 (2016).
4. Testa-Silva, G. *et al.* Human synapses show a wide temporal window for spike-timing-dependent plasticity. *Front. Synaptic Neurosci.* **2**, (2010).
5. Testa-Silva, G. *et al.* High bandwidth synaptic communication and frequency tracking in human neocortex. *PLoS Biol.* **12**, e1002007 (2014).
6. Eyal, G. *et al.* Unique membrane properties and enhanced signal processing in human neocortical neurons. *Elife* **5**, 2066 (2016).
7. Gidon, A. *et al.* Dendritic action potentials and computation in human layer 2/3 cortical

neurons. *Science* **367**, 83–87 (2020).

8. Huttenlocher, P. R. Synaptic density in human frontal cortex - developmental changes and effects of aging. *Brain Res* **163**, 195–205 (1979).
9. Kalmbach, B. E. *et al.* h-Channels Contribute to Divergent Intrinsic Membrane Properties of Supragranular Pyramidal Neurons in Human versus Mouse Cerebral Cortex. *Neuron* **100**, 1194-1208 e5 (2018).
10. Lourenço, J. & Bacci, A. Human-Specific Cortical Synaptic Connections and Their Plasticity: Is That What Makes Us Human? *PLoS Biol* **15**, 1–5 (2017).
11. Mansvelder, H. D., Verhoog, M. B. & Goriounova, N. A. Synaptic plasticity in human cortical circuits: cellular mechanisms of learning and memory in the human brain? *Curr. Opin. Neurobiol.* **54**, 186–193 (2019).
12. Mohan, H. *et al.* Dendritic and axonal architecture of individual pyramidal neurons across layers of adult human neocortex. *Cereb. Cortex* **25**, 4839–4853 (2015).
13. Sousa, A. M. M., Meyer, K. A., Santpere, G., Gulden, F. O. & Sestan, N. Evolution of the Human Nervous System Function, Structure, and Development. *Cell* **170**, 226–247 (2017).
14. Forrest, M. P., Parnell, E. & Penzes, P. Dendritic structural plasticity and neuropsychiatric disease. *Nat. Rev. Neurosci.* **19**, 215–234 (2018).
15. Krol, A. & Feng, G. Windows of opportunity: timing in neurodevelopmental disorders. *Curr. Opin. Neurobiol.* **48**, 59–63 (2018).
16. Mullins, C., Fishell, G. & Tsien, R. W. Unifying Views of Autism Spectrum Disorders: A Consideration of Autoregulatory Feedback Loops. *Neuron* **89**, 1131–1156 (2016).
17. Nelson, S. B. & Valakh, V. Excitatory/Inhibitory Balance and Circuit Homeostasis in Autism Spectrum Disorders. *Neuron* **87**, 684–698 (2015).
18. Tang, X., Jaenisch, R. & Sur, M. The role of GABAergic signalling in neurodevelopmental disorders. *Nat. Rev. Neurosci.* **22**, 290–307 (2021).
19. Dennis, M. Y. *et al.* The evolution and population diversity of human-specific segmental duplications. *Nat Ecol Evol* **1**, 69 (2017).
20. Dennis, M. Y. & Eichler, E. E. Human adaptation and evolution by segmental duplication. *Curr. Opin. Genet. Dev.* **41**, 44–52 (2016).
21. Liu, J., Mosti, F. & Silver, D. L. Human brain evolution: Emerging roles for regulatory DNA and RNA. *Curr. Opin. Neurobiol.* **71**, 170–177 (2021).
22. Pääbo, S. The human condition - A molecular approach. *Cell* **157**, 216–226 (2014).
23. Fossati, M. *et al.* SRGAP2 and Its Human-Specific Paralog Co-Regulate the Development of Excitatory and Inhibitory Synapses. *Neuron* **91**, 356–369 (2016).
24. Charrier, C. *et al.* Inhibition of SRGAP2 function by its human-specific paralogs induces neoteny during spine maturation. *Cell* **149**, 923–935 (2012).

25. Liu, X. *et al.* Extension of cortical synaptic development distinguishes humans from chimpanzees and macaques. *Genome Res.* **22**, 611–622 (2012).
26. Zhu, Y. *et al.* Spatiotemporal transcriptomic divergence across human and macaque brain development. *Science* **362**, eaat8077 (2018).
27. Dennis, M. Y. *et al.* Evolution of Human-Specific Neural SRGAP2 Genes by Incomplete Segmental Duplication. *Cell* 1–11 (2012).
28. Fortna, A. *et al.* Lineage-specific gene duplication and loss in human and great ape evolution. *PLoS Biol* **2**, E207 (2004).
29. Libé-Philippot, B. & Vanderhaeghen, P. Cellular and Molecular Mechanisms Linking Human Cortical Development and Evolution. *Annu. Rev. Genet.* **55**, 1–27 (2021).
30. Sudmant, P. H. *et al.* Diversity of human copy number variation and multicopy genes. *Science* **330**, 641–646 (2010).
31. Schmidt, E. R. E. *et al.* A human-specific modifier of cortical connectivity and circuit function. *Nature* **599**, 640–644 (2021).
32. Elston, G. N., Benavides-Piccione, R. & DeFelipe, J. The pyramidal cell in cognition: a comparative study in human and monkey. *J Neurosci* **21**, RC163 (2001).
33. Ho, C. *et al.* δ-Catenin is a nervous system-specific adherens junction protein which undergoes dynamic relocalization during development. *J. Comp. Neurol.* **420**, 261–276 (2000).
34. Zhou, J. *et al.* Presenilin 1 interaction in the brain with a novel member of the Armadillo family. *Neuroreport* **8**, 1489–1494 (1997).
35. Medina, M., Marinescu, R. C., Overhauser, J. & Kosik, K. S. Hemizygosity of δ-catenin (CTNND2) is associated with severe mental retardation in cri-du-chat syndrome. *Genomics* **63**, 157–164 (2000).
36. Turner, T. N. *et al.* Loss of δ-catenin function in severe autism. *Nature* **520**, 51–6 (2015).
37. van Rootselaar, A. F. *et al.* δ-Catenin (CTNND2) missense mutation in familial cortical myoclonic tremor and epilepsy. *Neurology* **89**, 2341–2350 (2017).
38. Israely, I. *et al.* Deletion of the Neuron-Specific Protein Delta-Catenin Leads to Severe Cognitive and Synaptic Dysfunction. *Curr. Biol.* **14**, 1657–1663 (2004).
39. Matter, C., Pribadi, M., Liu, X. & Trachtenberg, J. T. δ-Catenin Is Required for the Maintenance of Neural Structure and Function in Mature Cortex In Vivo. *Neuron* **64**, 320–327 (2009).
40. Arikkath, J. *et al.* Delta-catenin regulates spine and synapse morphogenesis and function in hippocampal neurons during development. *J. Neurosci.* **29**, 5435–5442 (2009).
41. Brigidi, G. S. *et al.* Palmitoylation of delta-catenin by DHHC5 mediates activity-induced synapse plasticity. *Nat. Neurosci.* 522–532 (2014).

42. Yuan, L., Seong, E., Beuscher, J. L. & Arikkath, J. δ-catenin regulates spine architecture via cadherin and PDZ-dependent interactions. *J. Biol. Chem.* **290**, 10947–10957 (2015).
43. Yuan, L. & Arikkath, J. Functional roles of p120ctn family of proteins in central neurons. *Semin. Cell Dev. Biol.* **69**, 70–82 (2017).
44. Coutinho-Budd, J., Ghukasyan, V., Zylka, M. J. & Polleux, F. The F-BAR domains from srGAP1, srGAP2 and srGAP3 regulate membrane deformation differently. *J. Cell Sci.* **125**, 3390–3401 (2012).
45. Koopmans, F. *et al.* SynGO: An Evidence-Based, Expert-Curated Knowledge Base for the Synapse. *Neuron* **103**, 217-234.e4 (2019).
46. Lu, Q., Aguilar, B. J., Li, M., Jiang, Y. & Chen, Y.-H. Genetic alterations of δ-catenin/NPRAP/Neurojungin (CTNND2): functional implications in complex human diseases. *Hum. Genet.* **135**, 1107–1116 (2016).
47. Krueger-Burg, D., Papadopoulos, T. & Brose, N. Organizers of inhibitory synapses come of age. *Curr. Opin. Neurobiol.* **45**, 66–77 (2017).
48. Sheng, M. & Hoogenraad, C. C. The postsynaptic architecture of excitatory synapses: a more quantitative view. *Annu Rev Biochem* **76**, 823–847 (2007).
49. Tyagarajan, S. K. & Fritschy, J.-M. Gephyrin: a master regulator of neuronal function? *Nat. Rev. Neurosci.* **15**, 141–156 (2014).
50. Chen, J. L. *et al.* Clustered Dynamics of Inhibitory Synapses and Dendritic Spines in the Adult Neocortex. *Neuron* **74**, 361–373 (2012).
51. Gemin, O. *et al. Unique properties of dually innervated dendritic spines in pyramidal neurons of the somatosensory cortex uncovered by 3D correlative light and electron microscopy*. *PLoS Biol* **19**, e3001375 (2021).
52. van Versendaal, D. *et al.* Elimination of Inhibitory Synapses Is a Major Component of Adult Ocular Dominance Plasticity. *Neuron* **74**, 374–383 (2012).
53. Lewis, A. S. *et al.* Alternatively spliced isoforms of TRIP8b differentially control h channel trafficking and function. *J. Neurosci.* **29**, 6250–6265 (2009).
54. Santoro, B., Wainger, B. J. & Siegelbaum, S. A. Regulation of HCN channel surface expression by a novel C-terminal protein-protein interaction. *J. Neurosci.* **24**, 10750–10762 (2004).
55. Zhang, X. *et al.* Deletion of the potassium channel Kv12.2 causes hippocampal hyperexcitability and epilepsy. *Nat. Neurosci.* **13**, 1056–1058 (2010).
56. Andrásfalvy, B. K., Makara, J. K., Johnston, D. & Magee, J. C. Altered synaptic and non-synaptic properties of CA1 pyramidal neurons in Kv4.2 knockout mice. *J. Physiol.* **586**, 3881–3892 (2008).
57. Gamache, T. R., Araki, Y. & Huganir, R. L. Twenty Years of SynGAP Research: From

Synapses to Cognition. *J Neurosci* **40**, 1596–1605 (2020).

58. Clement, J. P. *et al.* Pathogenic SYNGAP1 Mutations Impair Cognitive Development by Disrupting Maturation of Dendritic Spine Synapses. *Cell* **151**, 709–723 (2012).
59. Gross, G. G. *et al.* Recombinant probes for visualizing endogenous synaptic proteins in living neurons. *Neuron* **78**, 971–985 (2013).
60. Erzurumlu, R. S. & Gaspar, P. Development and critical period plasticity of the barrel cortex. *Eur J Neurosci* **25**, 1540–1553 (2012).
61. Kim, J. S. *et al.* Presenilin-1 inhibits δ-catenin-induced cellular branching and promotes δ-catenin processing and turnover. *Biochem. Biophys. Res. Commun.* **351**, 903–908 (2006).
62. Aceti, M. *et al.* Syngap1 haploinsufficiency damages a postnatal critical period of pyramidal cell structural maturation linked to cortical circuit assembly. *Biol. Psychiatry* **77**, 805–815 (2015).
63. Peixoto, R. T., Wang, W., Croney, D. M., Kozorovitskiy, Y. & Sabatini, B. L. Early hyperactivity and precocious maturation of corticostriatal circuits in Shank3B -/- mice. *Nat. Neurosci.* **19**, 716–724 (2016).
64. Hassani Nia, F. *et al.* Targeting of δ-catenin to postsynaptic sites through interaction with the Shank3 N-terminus. *Mol. Autism* **11**, 1–17 (2020).
65. Matsuda, T. & Cepko, C. L. Controlled expression of transgenes introduced by in vivo electroporation. *Proc. Natl. Acad. Sci. U. S. A.* **104**, 1027–1032 (2007).
66. Favuzzi, E. *et al.* Neurodevelopment: Distinct molecular programs regulate synapse specificity in cortical inhibitory circuits. *Science* **363**, 413–417 (2019).
67. Cong, L. *et al.* Multiplex Genome Engineering Using CRISPR/Cas Systems. *Science (80-.).* **339**, 819–823 (2013).
68. Fossati, M. *et al.* Trans-Synaptic Signaling through the Glutamate Receptor Delta-1 Mediates Inhibitory Synapse Formation in Cortical Pyramidal Neurons. *Neuron* **104**, 1081-1094 e7 (2019).
69. Meyer-Dilhet, G. & Courchet, J. In Utero Cortical Electroporation of Plasmids in the Mouse Embryo. *STAR Protoc.* **1**, 100027 (2020).
70. de Chaumont, F. *et al.* Icy: an open bioimage informatics platform for extended reproducible research. *Nat. Methods* **9**, 690–696 (2012).
71. Olivo-Marin, J. C. Extraction of spots in biological images using multiscale products. *Pattern Recognit.* **35**, 1989–1996 (2002).
72. Lagache, T. *et al.* Mapping molecular assemblies with fluorescence microscopy and object-based spatial statistics. *Nat. Commun.* **9**, 698 (2018).
73. Schindelin, J. *et al.* Fiji: an open-source platform for biological-image analysis. *Nat. Methods* **9**, 676–682 (2012).

74. Adesnik, H. & Scanziani, M. Lateral competition for cortical space by layer-specific horizontal circuits. *Nature* **464**, 1155–1160 (2010).
75. Vizcaíno, J. A. *et al.* 2016 update of the PRIDE database and its related tools. *Nucleic Acids Res.* **44**, D447--D456 (2016).
76. Poullet, P., Carpentier, S. & Barillot, E. myProMS, a web server for management and validation of mass spectrometry-based proteomic data. *Proteomics* **7**, 2553–2556 (2007).
77. Valot, B., Langella, O., Nano, E. & Zivy, M. MassChroQ: A versatile tool for mass spectrometry quantification. *Proteomics* **11**, 3572–3577 (2011).

FIGURE LEGENDS

Fig. 1. CTNND2 is a major interactor of SRGAP2 at synapses.

a, Schematic of the experimental workflow used for quantitative label-free mass spectrometry analysis. CoIP, co-immunoprecipitation; LC-MS/MS, liquid chromatography followed by tandem mass spectrometry.

b, Plot illustrating the partners of SRGAP2 identified in LC-MS/MS depending on their enrichment in SRGAP2 immunoprecipitate, adjusted p-value, and estimated abundance. Only proteins with > 15 peptides per 100 kDa are represented, data from 3 independent experiments.

c, SYNGO analysis of SRGAP2 interactome.

d, SRGAP2 partners involved in postsynaptic scaffolds and synaptic adhesion.

e, CTNND2-GFP co-immunoprecipitates with HA-tagged SRGAP2A and SRGAP2C in HEK cells.

f, Schematics of CTNND2, SRGAP2A and SRGAP2C protein domain structure. SRGAP2C lacks the last 49 amino-acids of the F-BAR domain of SRGAP2A and contains a few point mutations (*). CTNND2 interacts with both SRGAP2A and SRGAP2C.

Fig. 2. CTNND2 regulates excitatory and inhibitory synapses in opposite direction.

a, Confocal images of primary cortical neurons cultured for 18 days in vitro immunostained for endogenous CTNND2 and the excitatory or inhibitory postsynaptic markers PSD-95 and Gephyrin (GPHN). CTNND2 clusters associates with the majority of PSD-95 and Gephyrin clusters (arrowheads). Scale bar: 5 μm.

b, Boxplot with individual datapoints showing the fraction of PSD-95 or Gephyrin clusters associated with CTNND2 (association index). N_{PSD95} = 18; N_{GPHN} = 16 cells.

c, *In utero* electroporation (IUE) at embryonic day 14.5-15.5 allows the sparse targeting of layer 2/3 cortical pyramidal neurons (L2/3 CPN). Arrow indicates oblique apical dendrites. Scale bar: 50 μm.

d, Representative segments of dendrites expressing shControl, shCtnnd2, shCtnnd2 together with an shCtnnd2-resistant CTNND2* (rescue), or overexpressing CTNND2 (OE) along with mVenus in juvenile mice (P21-P23). Scale bar: 2 μm.

e, Quantifications of dendritic spine density in the conditions described in D. $N_{shControl}$ = 38; $N_{shCtnnd2}$ = 33; N_{Rescue} = 23; $N_{Ctnnd2\ OE}$ = 22 dendrites (1 dendrite per cell was analyzed). Dashed line indicates median of shControl condition.

f-g, Same as D-E but for gephyrin clusters in neurons expressing tdTomato to visualize neuronal contour (outlined by dashed lines) and EGFP-GPHN to visualize Gephyrin clusters. $N_{shControl}$ = 41; $N_{shCtnnd2}$ = 36; N_{Rescue} = 33; $N_{Ctnnd2\ OE}$ = 38. ns: $p > 0.05$; **: $p < 0.01$ and ***: $p < 0.001$, one-way ANOVA followed by Tukey's multiple comparisons test.

Fig. 3. CTNND2 deficiency increases the E/I ratio.

a, Schematic: recording of electroporated layer 2/3 CPN expressing tdTomato and the shRNA against CTNND2 (blue) following in utero electroporation (IUE) and neighboring non-electroporated control cells (gray) in acute brain slices from juvenile mice.

b, Representative traces of mEPSC and mIPSC recordings in control and shCtnnd2 electroporated neurons.

c-d, Quantification of mEPSC amplitude and frequency. In boxplots (left), data points represent mean values for individual cells. In scatterplots (right), data points show mean value from single pairs in which shCtnnd2 and control neurons were recorded from the same slice. N = 12 in both conditions.

e-f, Same as (**c-d**) for mIPSCs. N = 11 in both conditions.

g, Evoked postsynaptic currents were recorded in layer 2/3 CPNs by placing a stimulation electrode approximately 100 μm above the cell body along the apical dendrite.

h, Representative traces of eIPSCs and eEPSCs in control and shCtnnd2-expressing neurons.

i-j, E/I ratio calculated using the maximum amplitude or the synaptic charge. $N_{control}$ = 11 and $N_{shCtnnd2}$ = 16 cells.

Statistics: ns: $p > 0.05$; *: $p < 0.05$ and **: $p < 0.01$, Student t-test (**c-f**) or Mann-Whitney test (**i-j**).

Fig. 4. CTNND2 deficiency increases intrinsic excitability.

a-e, Quantification of intrinsic membrane properties in control and CTNND2-deficient neurons.

f, Traces of action potentials evoked at twice the rheobase by 1s depolarizing current steps in whole cell current clamp recordings.

g, CTNND2-deficient neurons fire action potentials at higher frequency than control neurons. $N_{control}$= 13 cells, $N_{shCtnnd2}$ = 16 cells. ns: $p > 0.05$; **: $p < 0,01$ and ***: $p < 0,001$, Student t-test.

Fig. 5. CTNND2 deficiency accelerates synaptic development and leads to spine loss in adults.

a-b, Representative segments of dendrites and quantification of spine density at indicated time points in neurons expressing shControl or shCtnnd2 and mVenus for visualization. P10: $N_{(control)}$ = 21, $N_{(shCtnnd2)}$ = 31; P21: $N_{(control)}$ = 38, $N_{(shCtnnd2)}$ = 33 (same as Fig. 2) ; P77: $N_{(control)}$ = 20, $N_{(shCtnnd2)}$ = 24. IUE: in utero electroporation. Scale bar: 2 μm.

c, Representative traces of mEPSCs recorded at P11.

d-e, Quantification of mEPSC amplitude and frequency in P9-11. In boxplots (left), data points represent mean values for individual cells. In scatterplots (right), data points show mean value from single pairs in which shCtnnd2 and control neurons were recorded from the same slice. N = 18 in each condition.

f-g, Evolution of mEPSC frequency over time (mean ± SEM).

h, Schematics of the biphasic effect of shCtnnd2 on synaptic excitation over time.

i, Experimental workflow of conditional knockdown experiments. All electroporated neurons are GFP-positive. ShControl or shCtnnd2 and mCherry expression is induced after tamoxifen injections between P28 and P31. Scale bar 50 μm.

j, Representative segments of dendrites and quantification of spine density in conditional knockdown experiments. $N_{(control)}$ = 22, $N_{(shCtnnd2)}$ = 25.

Statistics: ns: $p > 0.05$; *: $p < 0.05$; **: $p < 0.01$ and ***: $p < 0.001$; Student t-test or Kruskal-Wallis test with Dunn's multiple comparison test.

Fig. 6. CTNND2 interacts with key excitatory and inhibitory postsynaptic proteins and is regulated by SRGAP2C.

a, Schematic of the experimental workflow used for quantitative label-free mass spectrometry analysis.

b, Relative distribution and estimated abundance of proteins enriched in CTNND2 immunoprecipitates. Only proteins enriched at least 4 times, with at least 5 peptides, and whose p-value was < 0.05 based on three independent experiments are displayed. Cadherins and Catenins are shown in orange, SynGAP1 and Gephyrin (GPHN) are in red.

c, SYNGO gene ontology analysis of CTNND2 partners.

d, Classes of proteins and individual components standing out in CTNND2 protein complexes. Although not included in (**b**) due to our stringent threshold, GluA2 was also detected in CTNND2 complexes (3-fold enrichment, p = 0.007, 32 peptides / 100 kDa).

e, Representative dendritic segments and quantification of SYNGAP1 amount in spines of juvenile L2/3 CPNs expressing TdTomato and SynGAP1-GFP together with shControl or shCtnnd2 following in utero electroporation (IUE). $N_{shcontrol}$ = 17, $N_{shCtnnd2}$ = 20.

f, Same as E but for PSD-95 labelled with GFP-tagged FingRs. $N_{control}$ = 11 dendrites, $N_{shCtnnd2}$ = 10.

g, Representative dendritic segments and quantification of CTNND2 enrichment in spines in control and SRGAP2C-expressing neurons. $N_{control}$ = 16, $N_{SRGAP2C}$ = 16.

h, Representative dendritic segments and quantification of PSD-95 accumulation in spines in control and SRGAP2C-expressing neurons. $N_{control}$ = 17, $N_{SRGAP2C}$ = 24.

Statistics ns: $p > 0.05$; *: $p < 0.05$; ***: $p < 0,001$ Mann-Whitney test. One dendrite per cell was analyzed.

i, Model of CTNND2 and SRGAP2C-mediated regulation of synaptic maturation.

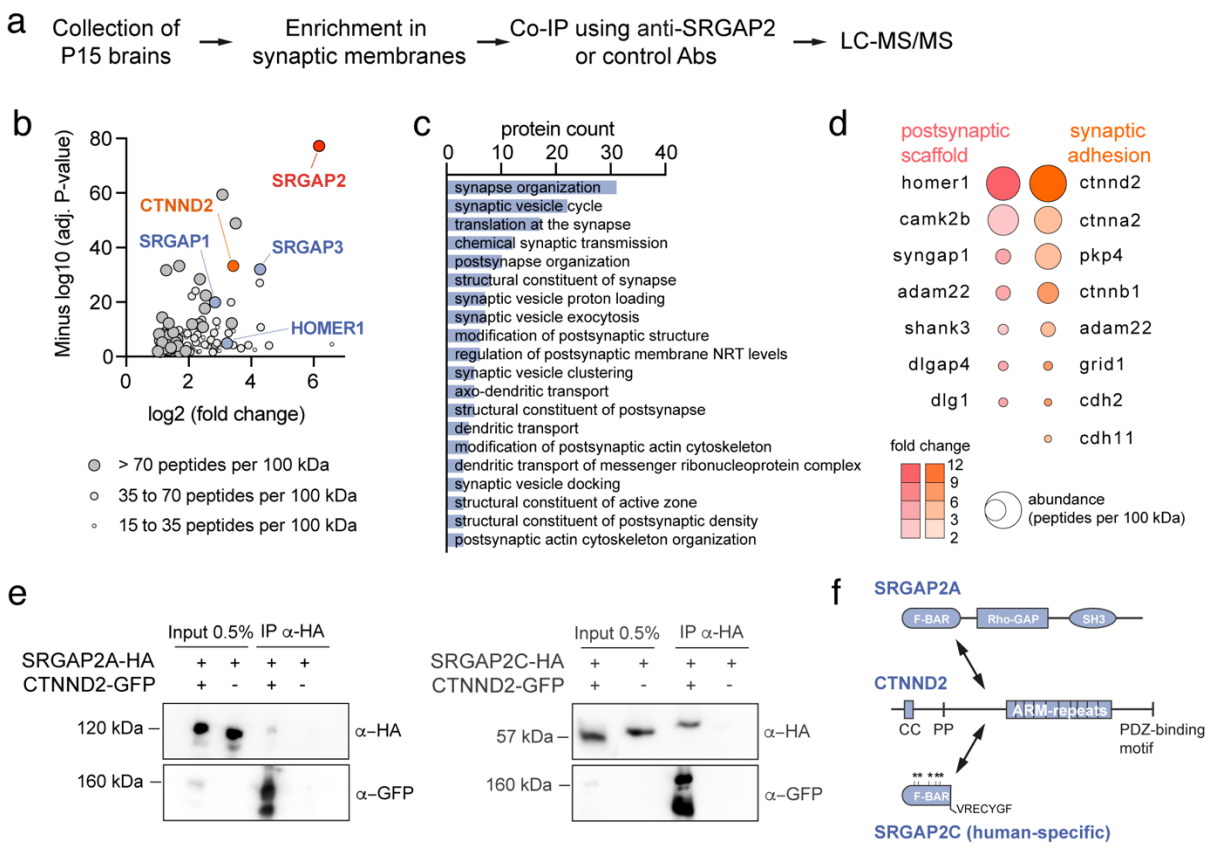
a
Collection of P15 brains
Enrichment in synaptic membranes
Co-IP using anti-SRGAP2 or control Abs
LC-MS/MS
b
Minus log10 (adj. P-value)
log2 (fold change)
SRGAP2
CTNND2
SRGAP1
SRGAP3
HOMER1
> 70 peptides per 100 kDa
35 to 70 peptides per 100 kDa
15 to 35 peptides per 100 kDa
c
protein count
synapse organization
synaptic vesicle cycle
translation at the synapse
chemical synaptic transmission
postsynapse organization
structural constituent of synapse
synaptic vesicle proton loading
synaptic vesicle exocytosis
modification of postsynaptic structure
regulation of postsynaptic membrane NRT levels
synaptic vesicle clustering
axo-dendritic transport
structural constituent of postsynapse
dendritic transport
modification of postsynaptic actin cytoskeleton
dendritic transport of messenger ribonucleoprotein complex
synaptic vesicle docking
structural constituent of active zone
structural constituent of postsynaptic density
postsynaptic actin cytoskeleton organization
d
postsynaptic scaffold
synaptic adhesion
homer1
camk2b
syngap1
adam22
shank3
dlgap4
dlg1
ctnnd2
ctnna2
pkp4
ctnnb1
adam22
grid1
cdh2
cdh11
fold change
abundance (peptides per 100 kDa)
e
Input 0.5%
IP α-HA
SRGAP2A-HA
CTNND2-GFP
120 kDa
160 kDa
α–HA
α–GFP
SRGAP2C-HA
57 kDa
f
SRGAP2A
F-BAR
Rho-GAP
SH3
CTNND2
CC
PP
ARM-repeats
PDZ-binding motif
VRECYGF
SRGAP2C (human-specific)

Figure 1

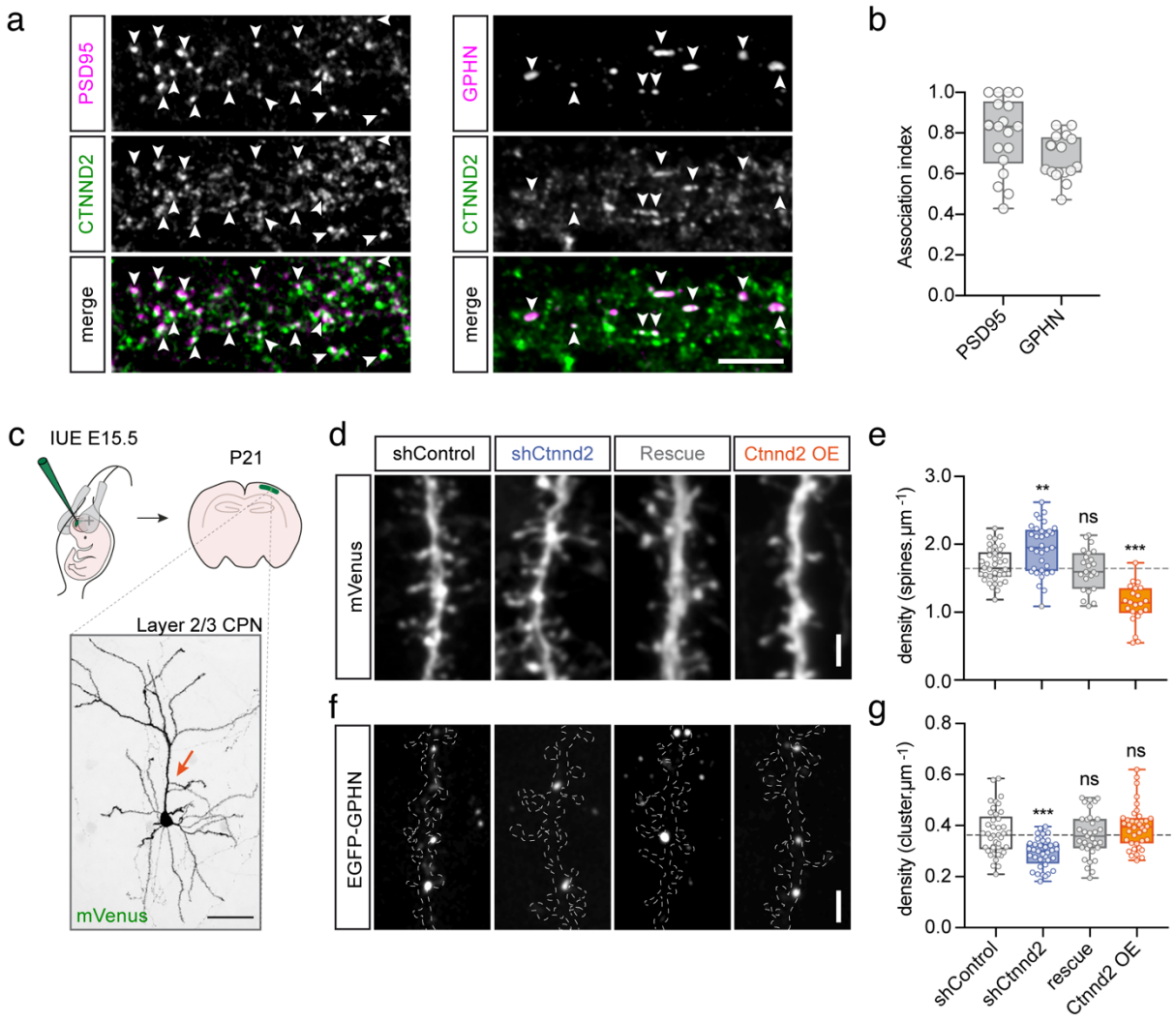
a
PSD95
CTNND2
merge
GPHN
CTNND2
merge
b
Association index
1.0
0.8
0.6
0.4
0.2
0.0
PSD95
GPHN
c
IUE E15.5
P21
Layer 2/3 CPN
mVenus
d
shControl
shCtnnd2
Rescue
Ctnnd2 OE
mVenus
e
density (spines.µm -1)
3.0
2.0
1.0
0.0
**
ns
***
f
EGFP-GPHN
g
density (cluster.µm -1)
0.8
0.6
0.4
0.2
0.0
***
ns
ns
shControl
shCtnnd2
rescue
Ctnnd2 OE

Figure 2

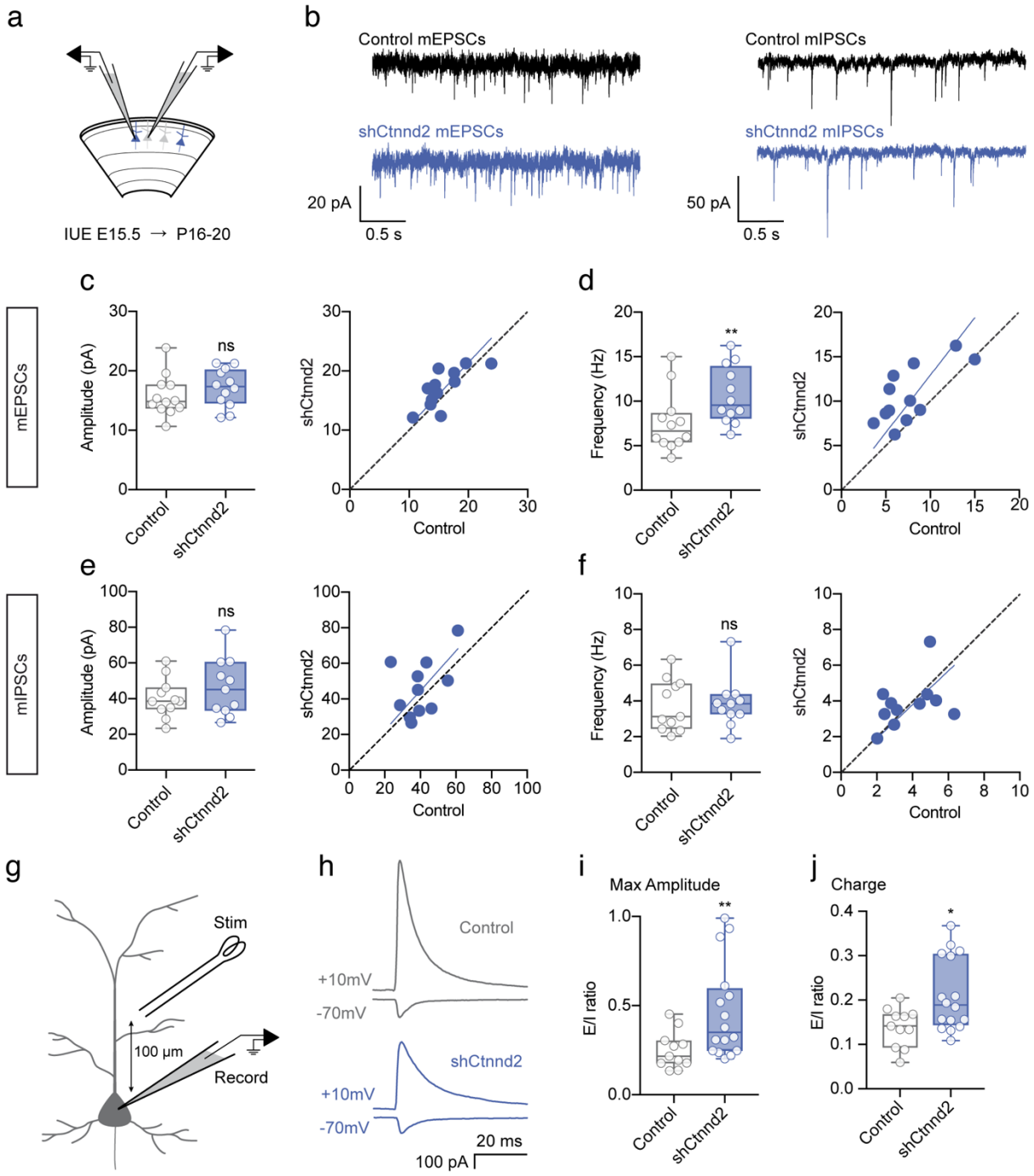
a
IUE E15.5 → P16-20
b
Control mEPSCs
shCtnnd2 mEPSCs
20 pA
0.5 s
Control mIPSCs
shCtnnd2 mIPSCs
50 pA
0.5 s
c
mEPSCs
Amplitude (pA)
ns
Control
shCtnnd2
shCtnnd2
Control
d
Frequency (Hz)
**
Control
shCtnnd2
shCtnnd2
Control
e
mIPSCs
Amplitude (pA)
ns
Control
shCtnnd2
shCtnnd2
Control
f
Frequency (Hz)
ns
Control
shCtnnd2
shCtnnd2
Control
g
Stim
100 µm
Record
h
Control
+10mV
-70mV
shCtnnd2
+10mV
-70mV
20 ms
100 pA
i
Max Amplitude
**
E/I ratio
Control
shCtnnd2
j
Charge
*
E/I ratio
Control
shCtnnd2

Figure 3

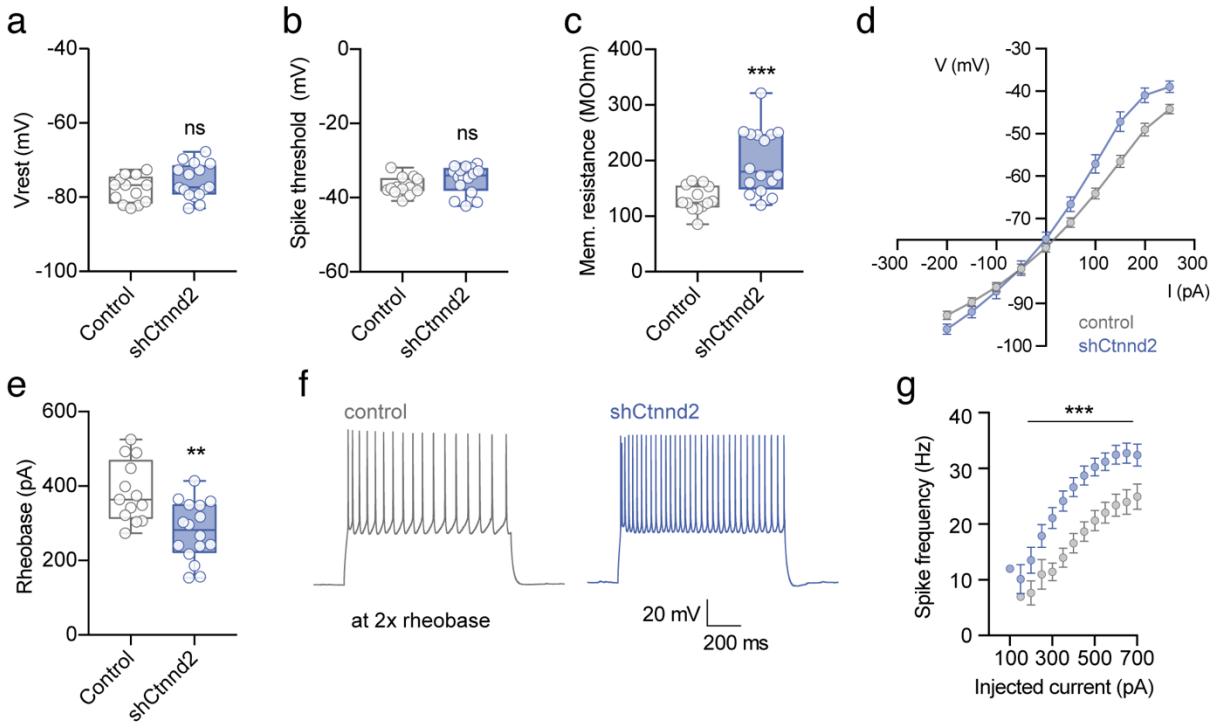
a
Vrest (mV)
-40
-60
-80
-100
ns
Control
shCtnnd2
b
Spike threshold (mV)
0
-20
-40
-60
ns
Control
shCtnnd2
c
Mem. resistance (MOhm)
400
300
200
100
0
***
Control
shCtnnd2
d
V (mV)
-30
-40
-50
-60
-70
-90
-100
-300 -200 -100
100 200 300
I (pA)
control
shCtnnd2
e
Rheobase (pA)
600
400
200
0
**
Control
shCtnnd2
f
control
shCtnnd2
at 2x rheobase
20 mV
200 ms
g
Spike frequency (Hz)
40
30
20
10
0
***
100 300 500 700
Injected current (pA)

Figure 4

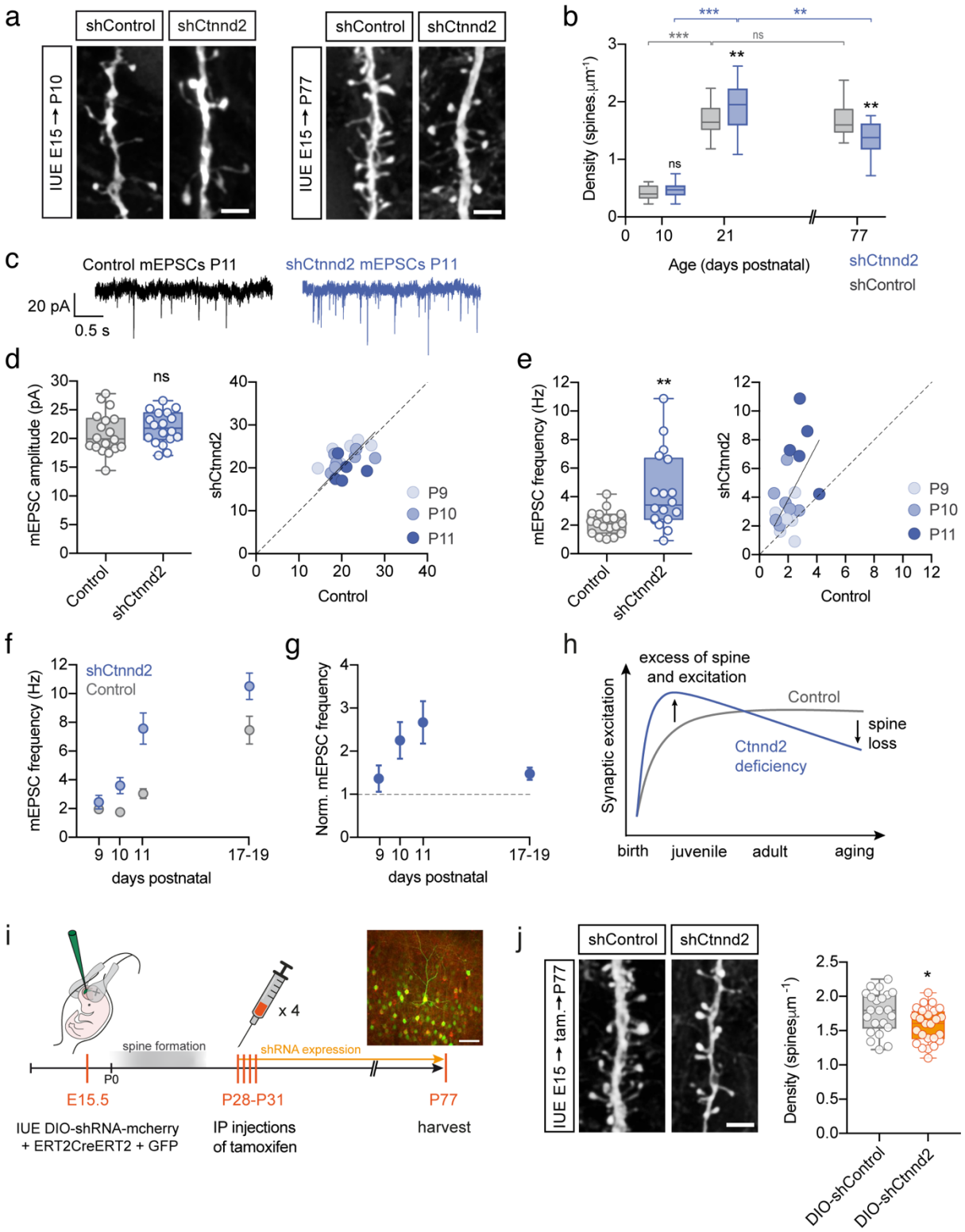
a
shControl
shCtnnd2
IUE E15 → P10
IUE E15 → P77
b
Density (spines.µm⁻¹)
Age (days postnatal)
shCtnnd2
shControl
c
Control mEPSCs P11
shCtnnd2 mEPSCs P11
20 pA
0.5 s
d
mEPSC amplitude (pA)
Control
shCtnnd2
P9
P10
P11
e
mEPSC frequency (Hz)
f
days postnatal
g
Norm. mEPSC frequency
h
excess of spine and excitation
Control
spine loss
Ctnnd2 deficiency
Synaptic excitation
birth
juvenile
adult
aging
i
spine formation
shRNA expression
x 4
E15.5
P28-P31
P77
IUE DIO-shRNA-mcherry + ERT2CreERT2 + GFP
IP injections of tamoxifen
harvest
j
IUE E15 → tam.→P77
DIO-shControl
DIO-shCtnnd2

Figure 5

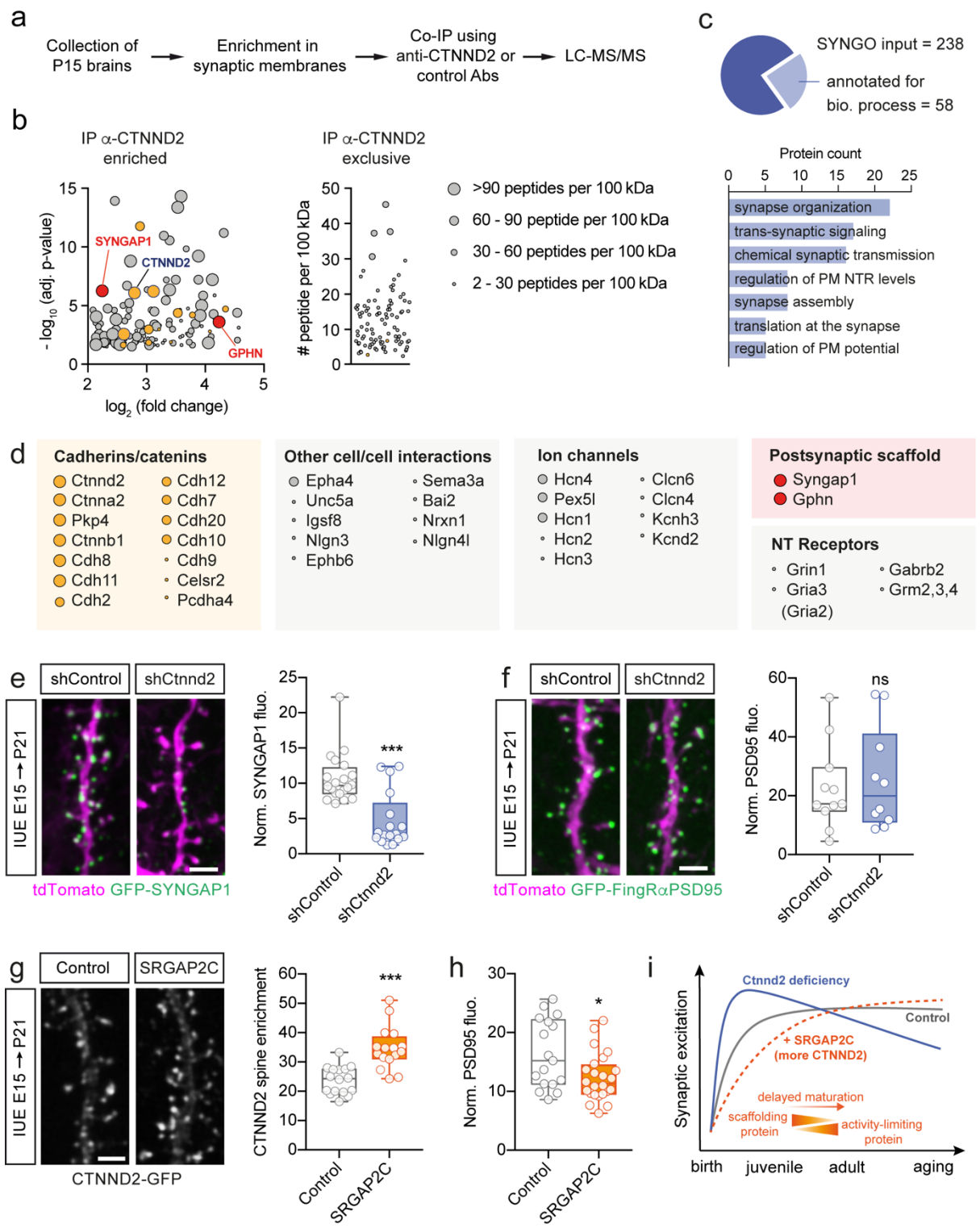
a
Collection of P15 brains
Enrichment in synaptic membranes
Co-IP using anti-CTNND2 or control Abs
LC-MS/MS
b
IP α-CTNND2 enriched
IP α-CTNND2 exclusive
- log10 (adj. p-value)
log2 (fold change)
SYNGAP1
CTNND2
GPHN
peptide per 100 kDa
>90 peptides per 100 kDa
60 - 90 peptide per 100 kDa
30 - 60 peptides per 100 kDa
2 - 30 peptides per 100 kDa
c
SYNGO input = 238
annotated for bio. process = 58
Protein count
synapse organization
trans-synaptic signaling
chemical synaptic transmission
regulation of PM NTR levels
synapse assembly
translation at the synapse
regulation of PM potential
d
Cadherins/catenins
Ctnnd2
Ctnna2
Pkp4
Ctnnb1
Cdh8
Cdh11
Cdh2
Cdh12
Cdh7
Cdh20
Cdh10
Cdh9
Celsr2
Pcdha4
Other cell/cell interactions
Epha4
Unc5a
Igsf8
Nlgn3
Ephb6
Sema3a
Bai2
Nrxn1
Nlgn4l
Ion channels
Hcn4
Pex5l
Hcn1
Hcn2
Hcn3
Clcn6
Clcn4
Kcnh3
Kcnd2
Postsynaptic scaffold
Syngap1
Gphn
NT Receptors
Grin1
Gria3 (Gria2)
Gabrb2
Grm2,3,4
e
shControl
shCtnnd2
IUE E15 → P21
tdTomato GFP-SYNGAP1
Norm. SYNGAP1 fluo.
***
f
tdTomato GFP-FingRαPSD95
Norm. PSD95 fluo.
ns
g
Control
SRGAP2C
CTNND2-GFP
CTNND2 spine enrichment
h
Norm. PSD95 fluo.
*
i
Ctnnd2 deficiency
Control
+ SRGAP2C (more CTNND2)
delayed maturation
scaffolding protein
activity-limiting protein
Synaptic excitation
birth
juvenile
adult
aging

Figure 6